Design of Graded Piezoelectric Metamaterial Beam with Spatial Variation of Electrodes

Yupei Jian[1], Lihua Tang[1]*, Guobiao Hu[2]*, Zhaoyu Li[1], Kean C Aw[1]

[1] Department of Mechanical Engineering, The University of Auckland, Auckland 1010, New Zealand
[2] School of Civil and Environmental Engineering, Nanyang Technological University, Singapore 639798, Singapore

*Correspondence authors: l.tang@auckland.ac.nz (Tang); guobiao.hu@ntu.edu.sg (Hu)

Abstract

This work presents a novel strategy of broadband vibration attenuation using a graded piezoelectric metamaterial beam. A series of electrode pairs with varying lengths are applied to the fully covered piezoelectric beam, and each electrode pair is connected to an identical shunt resonant circuit. Unlike the existing grading strategies, which normally consider the varying material properties of local resonators, the proposed graded metamaterial enables us to broaden the vibration attenuation region through varying spatial profiles. In this paper, the graded metamaterial beam is modeled analytically and verified by finite element. Subsequently, an analytical expression is derived to predict the "aggregated" gap region with graded electrodes. A parametric study on the transmittance response reveals that the increase of spatial variation of electrodes contributes to widening the attenuation region while weakening the attenuation strength. An optimization strategy aiming to enhance the overall attenuation performance is given, through which the graded piezoelectric metamaterial beam exhibits significant superiority over a non-graded one in terms of average transmittance. Further, an example shows that the damping induced by the load resistance in the shunt resonant circuit can dramatically reduce the resonant peaks inside the "aggregated" gap. With a properly selected resistance, a theoretical widest attenuation region is achieved by using the graded piezoelectric metamaterial beam, with 289.2% increase in the bandwidth as compared to the conventional one. This study differentiates itself as a powerful alternative to other grading strategies for realizing broadband vibration attenuation.

Keywords: Bandgap, graded piezoelectric metamaterial beam, shunt resonant circuit, broadband vibration attenuation

1. Introduction

Periodic structures are extensively studied in the applications for wave filtering [1-4] and vibration isolation [5, 6] due to the frequency bandgap in which waves can not propagate. The first mechanism that causes the bandgap phenomenon in periodic structures is known as Bragg Scattering [7]. Local resonance is the second mechanism for bandgap that is found in metamaterials, a type of periodic structure with locally resonating structures. Inspired by the concept of dynamic vibration absorbers [8], locally resonant metamaterial gives rise to the bandgap phenomenon at subwavelengths to attenuate low-frequency vibrations/noise. For example, recent research shows that elastic and acoustic waves can be attenuated simultaneously by using the design of local resonance-Helmholtz lattices [9]. However, the bandgap in the metamaterial with identical resonators is usually narrow [10] and attracts wide attention in the research community of metamaterial to widen the bandgap.

The design with multiple resonators has been proven to be influential for enlarging the vibration attenuation region, which can create multiple bandgaps by attaching independent single-degree-of-freedom resonators [11, 12]. Multiple bandgaps can also be achieved with multiple-degree-of-freedom resonators [13, 14]. By coupling the neighboring resonators using an internal spring, additional bandgaps could also be achieved [15]. Moreover, actively tunable metamaterials are appealing for broadband vibration control since the bandgap can be easily adjusted. As a typical tunable metamaterial, the piezoelectric metamaterial is fabricated by periodically bonding the substrated with piezoelectric patches connected to the shunt resonant circuits. The location and width of the bandgap can be tuned through the parameters in the shunt circuits and consequently the electromechanical coupling. Similar to the idea of multiple-degree-of-freedom mechanical resonators, the high-order shunt circuit technique [16] is adopted to generate multiple bandgaps and enlarge the attenuation region in piezeoelectric metamaterials. To date, feedback control circuits have been developed to enhance the piezoelectric coupling effect for wider bandgap [17-21], while the implementation complexity is inevitably increased. In addition, by combing the mechanical and electrical resonance mechanisms, two bandgaps corresponding to these two mechanisms could co-exist [22-25].

The aforementioned investigations were primarily devoted to strictly periodic structures with identical mechanical resonators (or shunt resonant circuits), which produce a bandgap limited to the bandwidth near the resonant frequency. However, the uncertainties in the

manufacturing processes would break the periodicity of the metamaterials required for the bandgap formation, which will result in the localization phenomenon [26, 27] and finally affect the vibration attenuation behavior. For example, the metamaterial with defect may exhibit waveguide modes within the bandgap. In the field of energy harvesting, by introducing piezoelectric patches to the defective metamaterial, wave localization can be exploited to collect energy [28]. Recently, graded metamaterials with near-periodic structures have attracted increasing interest due to its potential for broader attenuation bandwidth. "Graded" refers to the slight variation (usually formulated by a deterministic function) of the material/geometric properties of the cells. Banerjee et al. [29] studied a conceptual mass-in-mass represented metamaterial with slowly varying material properties. Significant enlargement of the attenuation region was achieved by using the grading strategy. Then, a more practical design, i.e., a graded metamaterial beam attached with mass-spring resonators, is proposed in [30]. With the proper arrangement of the natural frequencies of the resonators by varying stiffness, the attenuation bandwidth was increased by 172.5%, compared to the conventional metamaterial. Alshaqaq et al. [31] investigated a graded piezoelectric metamaterial beam with varying shunt inductance. Several grading patterns were proposed, and a 65% increase of the attenuation bandwidth was achieved compared to the design with identical shunt circuits. In addition. Celli et al. [32] studied the metamaterial with non-uniform spatial spacing between the local resonator, in which the disorder distribution of the resonators is beneficial for widening the attenuation bandwidth. However, the analysis by Sugino et al. in [33] showed the opposite findings and suggested that the non-uniformity should be avoided when they investigated the effect of the varying positioning of the resonators on the attenuation performance. Current understanding on the effect of varying spatial profiles on broadband vibration attenuation is still inadequate.

This work proposes a graded piezoelectric metamaterial beam with spatial variation of electrodes. The design criterion for the grading of the electrode pairs is derived, providing an alternative strategy for broadband vibration control using graded metamaterials. The remainder of this paper is organized as follows. **Section 2** presents the analytical model of the graded piezoelectric metamaterial beam with spatially varying electrodes, and the model validation using finite element (FE). In **Section 3**, the design criterion for the grading of the spatial variation of electrode pairs to avoid overturning is derived, and an analytical expression to predict the "aggregated" gap region is obtained. In **Section 4**, a comprehensive parametric study on the effect of the grading patterns is performed. An optimization strategy

to enhance the vibration attenuation performance in the targeted frequency range is considered. Additionally, an example is provided to show that the theoretical "aggregated" gap can be realized by adequately tuning the load resistance in the shunt resonant circuits to eliminate resonant peaks in the "aggregated" gap. Main conclusions from this work are summarized in **Section 5**.

2. Modelling of Graded Piezoelectric Metamaterial Beam

In this section, a theoretical model of the graded piezoelectric metamaterial beam is first established in Section 2.1, followed by the validation with finite element method in Section 2.2. This theoretical prediction of the transmittance will form the foundation to verify the design criterion of the proposed metamaterial beam in Section 3.

2.1 Theoretical Modeling

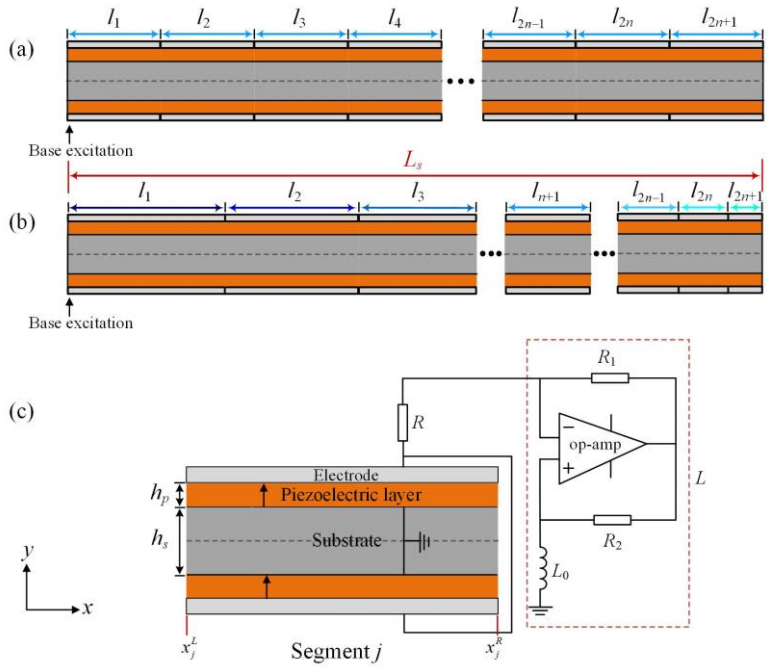

Figure 1. Sketches of (a) a conventional piezoelectric metamaterial beam, (b) a graded piezoelectric metamaterial beam with spatial variation of electrodes, and (c) an enlarged view of one beam segment shunted to an *L*-*R* circuit. The inductance *L* is achieved by the synthetic inductance circuit shown in the dashed box.

The conventional metamaterial beam covered with piezoelectric layers is shown in **Figure 1(a)**. The upper and lower piezoelectric layers are polarized in the same directions, with 2*n*+1 uniformly segmented electrodes. Each piezoelectric segment is connected to an identical *L*-*R* circuit, and an *L*-*C*-*R* resonant circuit is formed by coupling with the inherent capacitance of the piezoelectric segment. The *L*-*C*-*R* circuit can be treated as a local electromechanical

resonator with a fixed electrical resonant frequency, leading to a local resonance bandgap. The left-hand side of the piezoelectric metamaterial beam is clamped and subjected to the base excitation. A close view of one segment is shown in **Figure 1(c)**, in which the substrate and piezoelectric segments have the same length l and width b, and their thicknesses are h_s and h_p, respectively. The required inductance in each segment is fixed and achieved by the synthetic inductance circuit [34] shown in **Figure 1(c)**. The value of the inductance is determined by:

$$L = \frac{R_2}{R_1} L_0 \tag{1}$$

Figure 1(b) shows the proposed graded piezoelectric metamaterial beam with $2n+1$ pairs of spatially varying electrodes. Each pair of electrodes is connected to an identical shunt circuit. Instead of the same repetitive units, the electrode length in the x-direction, namely, l_j, j = 1, 2, …, $2n+1$, is intentionally altered by following a grading strategy. In this study, the effect of this spatial grading on vibration attenuation performance will be studied.

The graded piezoelectric metamaterial beam is assumed to be slender, and the rotary inertia and shear deformation are ignored. Applying the base excitation $w_b(t)=W_b e^{i\omega t}$ is conceptually equivalent to applying an acceleration field $a_{cc}=-\omega^2 W_b$. The transverse displacement $w(x,t)$ of the metamaterial beam relative to the base is governed by [35]:

$$EI\frac{\partial^4 w(x,t)}{\partial x^4} + m\frac{\partial^2 w(x,t)}{\partial t^2} = ma_{cc}e^{i\omega t} + \vartheta\sum_{j=1}^{2n+1} v_j(t)\frac{\partial^2}{\partial x^2}\left[H\left(x-x_j^L\right)-H\left(x-x_j^R\right)\right] \tag{2}$$

where $EI=E_sI_s+E_pI_p$ is the effective bending stiffness of the beam in short-circuit condition, in which E_s is the Young's modulus of the substrate and E_p is the Young's modulus of the piezoelectric layers in the short-circuit condition. $I_s = \frac{bh_s^3}{12}$ and $I_p = \frac{2b}{3}\left(\left(h_p+\frac{h_s}{2}\right)^3 - \frac{h_s^3}{8}\right)$ are the area moments of inertia of the substrate and the piezoelectric layer, respectively. $m = b\left(\rho_s h_s + 2\rho_p h_p\right)$ is the effective mass per unit length, in which ρ_s and ρ_p are the densities of subtrate and piezoelectric layers, respectively. $\vartheta = \frac{e_{31}b}{2h_p}\left[\left(h_p+\frac{h_s}{2}\right)^2 - \frac{h_s^2}{4}\right]$ is the electromechanical coupling term of the piezoelectric beam, where e_{31} is the effective piezoelectric stress constant. $v_j(t)$ is the voltage across the jth electrode pair. Due to the varying length of electrodes, $v_j(t)$ would be changed from segment to segment. To distinguish

the area covered by different electrodes, we multiply $[H(x-x_j^L)-H(x-x_j^R)]$ to the voltage term in Eq. (2), where x_j^L and x_j^R are the left and right ends of the *j*th electrode pairs and *H*(*) is the Heaviside function. The governing equation for the *j*th shunt circuit can be expressed as:

$$C_{p,j}\frac{dv_j(t)}{dt}+\Gamma\left[v_j(t)\right]+\vartheta\int_{x_j^L}^{x_j^R}\frac{\partial^3 w(x,t)}{\partial x^2\partial t}dx=0 \tag{3}$$

where $C_{p,j}=\dfrac{2\varepsilon_{33}^S b l_j}{h_p}$ and Γ are the inherent capacitance of the *j*th piezoelectric segment and a linear integrodifferential operator corresponding to the admittance shunted to each electrode pair, respectively. The two piezoelectric layers in each segment are electrically in parallel. Unlike previous works, we consider the piezoelectric metamaterial without strict geometric periodicity. The lattice constant in the conventional piezoelectric metamaterial no longer exists for the proposed beam. Before exploring the effect of the spatially graded electrodes on vibration attenuation, we first define a constant spatial variation between adjacent cells as:

$$\delta=\frac{l_j-l_{n+1}}{j-(n+1)} \tag{4}$$

Here, to ensure a uniform variation of electrodes, the length of (*n*+1)th electrode, i.e., the electrode in the middle of the piezoelectric metamaterial beam, is chosen as the average length:

$$l_{n+1}=\frac{L_\mathrm{s}}{2n+1} \tag{5}$$

where L_s is the length of the substrate. By substituting Eq. (5) into Eq. (4), the length of the *j*th electrode can be obtained as:

$$l_j=x_j^R-x_j^L=\delta(j-n-1)+\frac{L_\mathrm{s}}{2n+1} \tag{6}$$

where the coordinates of the two ends of the *j*th electrode are $x_j^L=\sum_{h=1}^{j}(l_h)-l_j$ and $x_j^R=\sum_{h=1}^{j}l_h$.

By inserting Eq. (6) into the expression of $C_{p,j}$, $C_{p,j}$ can be written in terms of $C_{p,n+1}$ as:

$$C_{p,j}=\left(\frac{\delta(j-n-1)(2n+1)}{L_\mathrm{s}}+1\right)C_{p,n+1} \tag{7}$$

where $C_{p,n+1}$ is the inherent capacitance of the (n+1)th piezoelectric segment. Note that for each cell, an identical series *L*-*R* circuit is connected to the piezoelectric segment, forming a *L*-*C*-*R* circuit. The resonant frequency of the *j*th *L*-*C*-*R* circuit is $\omega_j = \sqrt{1/\left(LC_{p,j}\right) - \left(R/L\right)^2}$. Since inherent capacitance $C_{p,j}$ is very small, the second-order term $\left(R/L\right)^2$ is negligible as compared to the first-order term $1/\left(LC_{p,j}\right)$. Therefore, the resonant frequency $\omega_{LC,j}$ is approximated to be $\omega_{LC,j} = \sqrt{1/\left(LC_{p,j}\right)}$ to simplify the derivation. Considering Eq. (7), one can obtain the resonant frequency of the *j*th shunt circuit in terms of $\omega_{LC,n+1}$:

$$\omega_{LC,j} = \frac{1}{\sqrt{\dfrac{\delta\left(j-n-1\right)\left(2n+1\right)}{L_s}+1}}\omega_{LC,n+1} \tag{8}$$

Eq. (8) implies that $\omega_{LC,j}$ would vary from segment to segment, and the variation depends on the values of δ and n.

By using the modal superposition method, the transverse vibration of the beam relative to the base is expressed as the summation of N truncated modes:

$$w(x,t) = \sum_{k=1}^{N} \phi_k(x)\eta_k(t) \ \ (k = 1,2,3...) \tag{9}$$

where $\phi_k(x)$ and $\eta_k(t)$ are the *k*th mode shape and modal coordinate of the piezoelectric metamaterial beam in the short-circuit condition, respectively. $\phi_k(x)$ are mass-normalized using the orthogonality conditions below:

$$\int_0^{L_s} m\phi_k(x)\phi_r(x)dx = \delta_{kr} \tag{10}$$

$$\int_0^{L_s} EI\frac{d^4\phi_k(x)}{dx^4}\phi_r(x)dx = \int_0^{L_s} EI\frac{d^2\phi_k(x)}{dx^2}\frac{d^2\phi_r(x)}{dx^2}dx = \omega_k^2\delta_{kr} \tag{11}$$

Under the harmonic base excitation, $\eta_k(t)$ is in the form of $\eta_k(t) = \bar{\eta}_k e^{i\omega t}$, where $\bar{\eta}_k$ denotes the steady-state amplitude of the *k*th modal coordinate. By inserting Eq. (9) into Eq. (3) and then applying Laplace transform, we obtain:

$$\bar{v}_j = -\frac{i\omega\vartheta\sum_{k=1}^{N}\Delta\dfrac{d\phi_k\left(x_j\right)}{dx}\bar{\eta}_k}{\dfrac{1}{R+i\omega L}+i\omega\left(\dfrac{\delta\left(j-n-1\right)\left(2n+1\right)}{L_s}+1\right)C_{p,n+1}} \tag{12}$$

where $\bar{v}_j$ is the steady-state voltage amplitude across the *j*th electrode pair, and $\Delta\dfrac{d\phi_k\left(x_j\right)}{dx}=\dfrac{d\phi_k\left(x_j^R\right)}{dx}-\dfrac{d\phi_k\left(x_j^L\right)}{dx}$. Substituting Eqs. (9) and (12) into the Eq. (2), multiplying by $\phi_r(x)$, integrating over the length of the beam from 0 to L_s, applying the orthogonality conditions, and introducing modal damping, we can obtain the modal governing equation as:

$$\bar{\eta}_r+\sum_{j=1}^{2n+1}\frac{i\omega\vartheta^2\dfrac{1}{\left(\omega_r^2+2i\omega\zeta_r\omega_r-\omega^2\right)}}{\dfrac{1}{R+i\omega L}+i\omega\left(\dfrac{\delta\left(j-n-1\right)\left(2n+1\right)}{L_s}+1\right)C_{p,n+1}}\Delta\frac{d\phi_r\left(x_j\right)}{dx}\sum_{k=1}^{N}\Delta\frac{d\phi_k\left(x_j\right)}{dx}\bar{\eta}_k=\frac{ma_{cc}\int_0^{L_s}\phi_r(x)\,dx}{\left(\omega_r^2+2i\omega\zeta_r\omega_r-\omega^2\right)} \tag{13}$$

where ζ_r is the modal damping ratio.

Rearranging Eq. (13) in the term of $\bar{\eta}_r$ gives:

$$\mathbf{C}\boldsymbol{\eta}=\mathbf{F} \tag{14}$$

where

$$\mathbf{C}=\begin{bmatrix} c_{11} & c_{12} & \cdots & c_{1m} & \cdots & c_{1N} \\ c_{21} & c_{22} & \cdots & c_{2m} & \cdots & c_{2N} \\ \cdots & \cdots & \cdots & \cdots & \cdots & \cdots \\ c_{r1} & c_{r2} & \cdots & c_{rm} & \cdots & c_{rN} \\ \cdots & \cdots & \cdots & \cdots & \cdots & \cdots \\ c_{N1} & c_{N2} & \cdots & c_{Nm} & \cdots & c_{NN} \end{bmatrix} \quad \boldsymbol{\eta}=\begin{bmatrix} \bar{\eta}_1 \\ \bar{\eta}_2 \\ \cdots \\ \bar{\eta}_r \\ \cdots \\ \bar{\eta}_N \end{bmatrix} \quad \mathbf{F}=\begin{bmatrix} f_1 \\ f_2 \\ \cdots \\ f_r \\ \cdots \\ f_N \end{bmatrix} \tag{15}$$

and

$$c_{r,m}=\begin{cases} 1+\displaystyle\sum_{j=1}^{2n+1}\frac{i\omega\vartheta^2\dfrac{1}{\left(\omega_r^2+2i\omega\zeta_r\omega_r-\omega^2\right)}}{\dfrac{1}{R+i\omega L}+i\omega\left(\dfrac{\delta\left(j-n-1\right)\left(2n+1\right)}{L_s}+1\right)C_{p,n+1}}\Delta\frac{d\phi_r\left(x_j\right)}{dx}\Delta\frac{d\phi_m\left(x_j\right)}{dx}, \text{ for } m=r \\ \displaystyle\sum_{j=1}^{2n+1}\frac{i\omega\vartheta^2\dfrac{1}{\left(\omega_r^2+2i\omega\zeta_r\omega_r-\omega^2\right)}}{\dfrac{1}{R+i\omega L}+i\omega\left(\dfrac{\delta\left(j-n-1\right)\left(2n+1\right)}{L_s}+1\right)C_{p,n+1}}\Delta\frac{d\phi_r\left(x_j\right)}{dx}\Delta\frac{d\phi_m\left(x_j\right)}{dx}, \text{ for } m\neq r \end{cases} \tag{16}$$

and

$$f_r=\frac{ma_{cc}\int_0^{L_s}\phi_r(x)\,dx}{\omega_r^2+2i\omega\zeta_r\omega_r-\omega^2} \tag{17}$$

Solving Eq. (14) to obtain $\boldsymbol{\eta}$, and substituting it back to Eq. (9), one can calculate $W\left(x,\omega\right)$, which is the steady-state deflection amplitude of the beam relative to the base. Then, the

transmittance of the graded metamaterial beam is defined to evaluate the vibration attenuation performance as follows:

$$\tau(\omega) = 20\log\left(\frac{\left|W_{abs}(L_s,\omega)\right|}{\left|W_b(\omega)\right|}\right)\text{dB} \tag{18}$$

where $W_{abs}(L_s,\omega) = W(L_s,\omega) + W_b(\omega)$ denotes absolute steady-state displacement amplitude at the beam tip. $\tau(\omega) < 0$ indicates that the tip displacement is smaller than the excitation amplitude, implying that the vibration is suppressed.

2.2 Model Validation

To validate the theoretical model presented in Section 2.1, the graded piezoelectric metamaterial beam with spatially varied electrodes is modeled and simulated using the finite element package COMSOL Multiphysics. An aluminum substrate and two PZT-5H layers are considered. **Table 1** lists the geometric and material properties of the system.

Table 1. Geometric and material properties of piezoelectric metamaterial beam

Substrate	
Material	Aluminum
Density ρ_s	2700 kg/m^3
Young's modulus E_s	69 GPa
Thickness h_s	1 mm
Width b	10 mm
Total Length L_s	440 mm
Piezoelectric layer	
Material	PZT-5H
Young's modulus in short-circuit condition E_p	60.6 GPa
Density ρ_p	7500 kg/m^3
Piezoelectric coefficient e_{31}	-16.61 C/m^2
Permittivity ε_{33}^S	2.5554e-08 F/m
Thickness h_p	0.3 mm

Two grading patterns, i.e., $\delta = \pm 0.001$ with 11 electrodes (n = 5) on the top and bottom surfaces of the piezoelectric layers, are adopted. An identical shunt circuit formed by a synthetic inductor L = 37.2 H in series with the resistance R = 50 Ω is connected to the electrodes of each cell, as shown in **Figure 1(c)**. In addition, the 3D piezoelectric constitutive relation is reduced to 1D in COMSOL to ensure consistency with the theoretical model for

the transducer operating in 31-mode. The elastic matrix $\mathbf{C_E}$ and coupling matrix $\mathbf{e}$ of the piezoelectric material in COMSOL are defined as:

$$\mathbf{C_E}=E_p\mathbf{I}_{6\times6},\quad \mathbf{e}=\begin{bmatrix}\mathbf{0} & \mathbf{0}\\ e_{31} & \mathbf{0}\end{bmatrix},\quad \boldsymbol{\varepsilon}^{\mathbf{S}}=\left[0,0,\varepsilon_{33}^{S}\right] \tag{19}$$

where $\mathbf{I}$ is an identity matrix. By exerting a displacement excitation to the base, the transmittance can be calculated by measuring the tip displacement of the piezoelectric beam. **Figure 2** compares the theoretical and FE results of the transmittance of the proposed graded beam, and good agreement is observed.

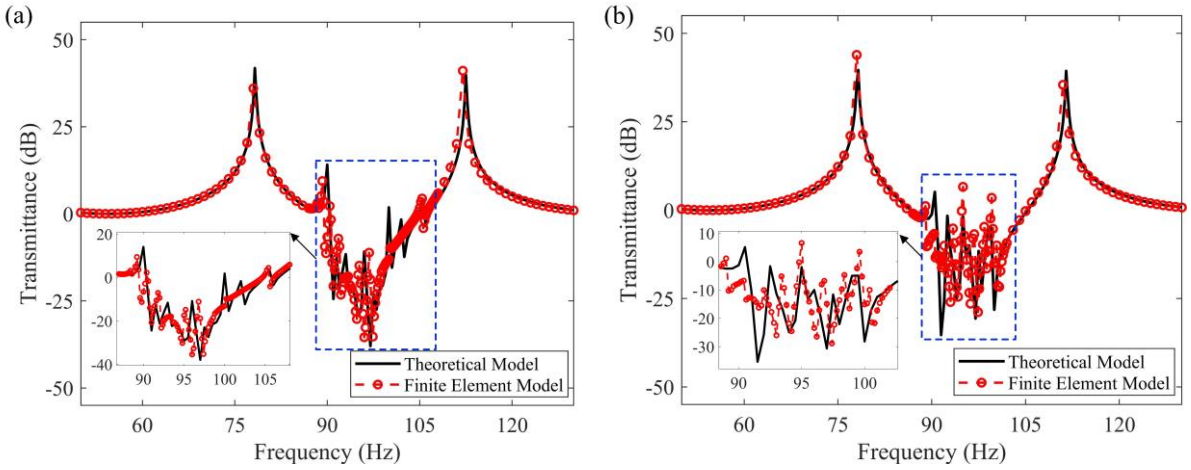

Figure 2. Comparison of theoretical and FE results of the transmittance of the graded piezoelectric metamaterial beam with (a) δ = 0.001 and (b) δ = −0.001. n = 5, L = 37.2 H, and R = 50 Ω are used.

3. Design of Graded Piezoelectric Metamaterial Beam

In our previous study [36], by seeking the extreme points of the band structure of the infinitely long model of a piezoelectric metamaterial beam, we have derived its bandgap range ("BG" for short):

$$\text{BG: } \alpha\omega_{LC} < \omega < \omega_{LC} \tag{20}$$

where the constant coefficient $\alpha=\sqrt{\dfrac{\left(1-k_{31}^2\right)E_pI_p+E_sI_s}{E_pI_p+E_sI_s}}$ stands for the square root of the ratio of the effective bending stiffnesses in short-circuit and open-circuit conditions. Eq. (20) has been verified to provide high accuracy in [36]. From this expression, it is observed that the upper bound of the bandgap is located at the resonant frequency ω_{LC} of the L-C shunt

resonant circuit. In addition, the bandgap can be extended toward low frequencies by tuning α, which is less than 1 and depends on the electromechanical coupling coefficient of the piezoelectric material k_{31}. However, for common piezoelectric materials, k_{31} is generally small and much less than 1 [37]. As a result, the coefficient α is close to 1, and the bandgap generated by the piezoelectric shunt resonant circuit is usually very narrow.

For the proposed piezoelectric metamaterial beam with spatially varying electrodes, the intentionally changed length of electrodes would modify the value of the inherent capacitances of different piezoelectric segments. Based on Eq. (8), the $2n$+1 pieces of piezoelectric segments will be assigned with a series of different resonant frequencies, i.e., $\omega_{LC,1}, \omega_{LC,2} ... \omega_{LC,2n+1}$. A constant spatial variation δ has been defined to tune these resonant frequencies in a "graded" manner. Ideally, by perfectly jointing these discrete bandgaps, an "aggregated" gap would be formed, allowing the possibility to achieve wave attenuation in a broad frequency range. According to Eq. (8), positive δ means the electrode length increases along the x-direction, leading to the resonant frequencies arranged in the descending order, i.e., $\omega_{LC,1} > \omega_{LC,2} > ... > \omega_{LC,n+1} > ... > \omega_{LC,2n+1}$. In this case, the bandgap range becomes $\mathrm{BG}_{2n+1}^{-} < \omega < \mathrm{BG}_{1}^{+}$, where BG_{2n+1}^{-} denotes the lower bound of the bandgap of the (2n+1)th segment and BG_{1}^{+} denotes the upper bound of the first segment. When δ is negative, the distribution pattern of electrodes is precisely the opposite: negative δ indicates the shrink of electrodes along the x-direction, leading to the resonant frequencies evolve in the ascending order, i.e., $\omega_{LC,1} < \omega_{LC,2} < ... < \omega_{LC,n+1} < ... < \omega_{LC,2n+1}$. Accordingly, the "aggregated" gap can be predicted as $\mathrm{BG}_{1}^{-} < \omega < \mathrm{BG}_{2n+1}^{+}$. It is worth mentioning that changing the sign of δ does not affect the division of the piezoelectric segments for deploying electrode pairs, and it only indicates arranging the electrode pairs starting from the other end of the beam. Hence, the resonant frequency $\omega_{LC,n+1}$ of the (n+1)th segment is always at the center of the resonant frequency array $\omega_{LC,1}, \omega_{LC,2} ... \omega_{LC,2n+1}$, irrespective of the sign of δ. By considering Eq. (20), one can predict the "aggregated" gap in terms of $\omega_{LC,n+1}$ as:

$$\frac{\alpha}{\sqrt{1+(-1)^p \dfrac{\left(2n^2+n\right)\delta}{L_s}}} \omega_{LC,n+1} < \omega < \frac{1}{\sqrt{1-(-1)^p \dfrac{\left(2n^2+n\right)\delta}{L_s}}} \omega_{LC,n+1} \tag{21}$$

where p=1 for the case of $\delta < 0$ and p=2 for the case of $\delta > 0$. Note that theoretically, the sign change of δ will not affect the gap's width. The discrepancy in the effect of the positive and negative δ on vibration suppression performance will be discussed in Section 4.1.

In some circumstances, the adjacent bandgaps may be completely separated, thus invalidating Eq. (21) and must be avoided from the perspective of broadband vibration attenuation. Therefore, it is necessary to set the criterion for selecting δ. To better study the effect of δ on the discrete bandgaps, we first define a dimensionless parameter to describe the frequency spacing between the neighboring bandgaps:

$$\Delta\Omega_j = \frac{\mathrm{BG}_j^- - \mathrm{BG}_{j+1}^+}{\mathrm{BG}_{n+1}}, \quad \delta > 0 \tag{22}$$

$\Delta\Omega_j > 0$ means two neighboring bandgaps are separated. $\Delta\Omega_j < 0$ indicates that the jth and (j+1)th bandgaps are overlapped and $\Delta\Omega_j$ is termed as "overlap zone". The criteria of δ should guarantee that $\Delta\Omega_j$ is the overlap zone for any j. **Figure 3** demonstrates the variation of $\Delta\Omega_j$ with j. Notably, only positive δ is considered here, since the resultant curves with $\pm\delta$ are symmetric with respect to the vertical axis. In this numeric example, the length of the substrate is set to be L_s = 440 mm, and the number of electrodes is 11, respectively. Different δ are used for demonstration. It can be seen that for $\delta > 0$, $\Delta\Omega_j$ decreases monotonically as j increases. The frequency spacing of neighboring bandgaps for three cases (i.e., a, b, and c) are also shown in **Figure 3.**

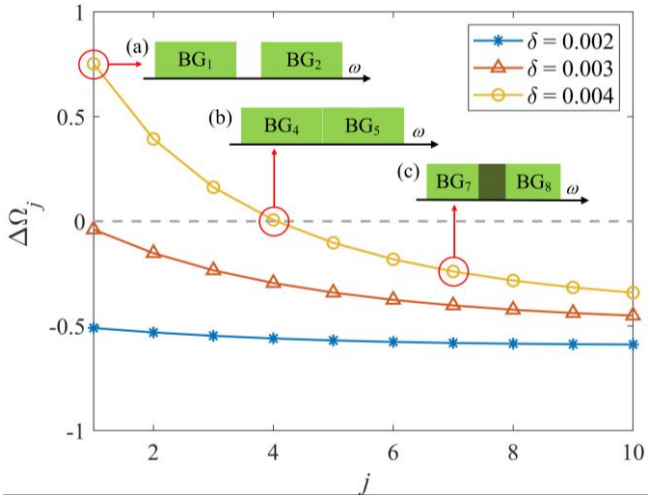

Figure 3. Variation of the bandgap interval $\Delta\Omega_j$ along with j. Note that $\Delta\Omega_j < 0$ indicates that the jth and (j+1)th bandgaps are overlapped. For δ = 0.004, the subplots when j = 1, 4 and 7, respectively represent three cases of frequency spacing of neighboring bandgaps: (a) without overlapping; (b) perfect jointing; (c) overlapping.

As long as the $\Delta\Omega_1 < 0$, it is guaranteed that all $\Delta\Omega_j < 0$, i.e., the design basis is:

$$\mathrm{BG}_1^- \le \mathrm{BG}_2^+ \tag{23}$$

By considering the symmetricity, the following inequality should be satisfied for negative δ:

$$\mathrm{BG}_{2n}^+ \ge \mathrm{BG}_{2n+1}^- \tag{24}$$

Combining Eqs. (8) and (20) with Eqs. (23) and (24), one can obtain:

$$|\delta| \le \frac{L_s\left(1-\alpha^2\right)}{\left(2n+1\right)\left(\alpha^2\left(1-n\right)+n\right)} \tag{25}$$

Eq. (25) is a design criterion for acquiring the "aggregated" gap estimated by Eq. (21). Note that the constrained range of δ is only related to the number of electrodes, the length of the substrate, and the constant coefficient α. It is worth mentioning that the bandgap bound equation of the conventional metamaterial (i.e., Eq. (20)) is derived based on the assumption of an infinitely periodic metamaterial beam. While, for the non-uniform finitely long beam, though an overall wider attenuation region is covered, the scattered gap ranges produced by each segment will undoubtedly weaken the vibration attention strength. As a result, it might not be able to suppress the resonant peaks, and the actual attenuation range might be lower than the designed "aggregated" gap. The fidelity of Eq. (21) will be discussed in Section 4.3.

4. Results and Discussions

In this section, based on the developed model in Section 2.1, and the design criterion derived in Section 3, we thoroughly study the attenuation performance of the proposed graded metamaterial beam. This section commences with investigating the effect of the spacing variation δ on the attenuation region (Section 4.1), and then illustrates the superiority of the graded metamaterial over the conventional counterpart (Section 4.2). Some undesired characteristics brought by the grading design are discussed in Section 4.3.

4.1 Effect of δ on Attenuation Region

This subsection aims to investigate the evolution of attenuation region with the variation of δ. Without loss of generality, two cases, i.e., n = 5 and 10 are chosen, corresponding to 11 and 21 pairs of electrodes, respectively. The geometric and material parameters listed in **Table 1** are used. Based on these parameters, the coefficient α in Eq. (20) can be calculated as α =

0.9431. According to Eq. (25), the criteria of δ are determined as $|\delta| \le 0.00306$ and $|\delta| \le 0.00116$, corresponding to n = 5 and n = 10, respectively. A load resistance (R = 50 Ω) is chosen for each shunt resonant circuit to add some damping. The effect of load resistance will be discussed in Section 4.3. **Figure 4** shows the attenuation heatmaps by varying the spatial variation δ. The colored areas correspond to transmittance $\tau(\omega) < 0$ and the darker the color, the stronger the attenuation. For n = 5, based on Eq. (5), the length of the (n+1)th electrode of the middle segment is l_{n+1} = 40 mm. Three different values of inductor L, i.e., L = 37.17 H, L = 2.32 H, and L = 0.76 H are considered, leading to the resonant frequency of the (n+1)th shunt circuit being f_{n+1} = 100 Hz, 400 Hz, and 700 Hz, respectively. The evolution trend of attenuation region (i.e., $\tau(\omega) < 0$) is shown in **Figure 4(a), (b)** and **(c)**. The two dashed lines correspond to the "aggregated" gap range estimated by Eq. (21), which are generally consistent with the attenuation heatmap contours. It is noted that, with the introduction of grading ($\delta \neq 0$), the attenuation region is expanded toward high and low frequencies as compared to the case without "grading" (δ = 0), while the colored region becomes lighter with the increase of $|\delta|$. It is also noted that the attenuation region begins to scatter (blank areas appear) with the increase of $|\delta|$, especially when $|\delta|$ approaches the threshold of the design criterion ($|\delta| \le 0.00306$). This can be attributed to the scattered resonant frequencies of the shut circuits leading to a weaker suppression strength, and the intended overlap of discrete bandgaps in the design stage can not be guaranteed. Consequently, multiple unexpected resonant peaks inside the intended "aggregated" gap emerge. It is also observed that this phenomenon is particularly pronounced at low-frequency case (f_{n+1} = 100 Hz), which can be explained by the fact that vibration attenuation is more challenging at low-frequency region than at high-frequency region. In other words, the piezoelectric segment connected to the shunt circuit with a lower resonant frequency has a relatively weaker vibration suppression capability, especially in terms of the bandgap width [38]. The unexpected resonant peaks are also known as localization [39, 40], normally occur in some near-periodic structures with slowly varying material/geometric properties. Physically, a few transverse waves with frequencies inside the predicted bandgap region are not attenuated but rather reflected and propagated along the opposite direction. In some literature on metamaterials-based energy harvesting, researchers have taken advantage of the localized mode to harvest the vibration energy over a wider frequency range [41]. However, this phenomenon is undesired from the perspective of broadband vibration attenuation. A

decent damping should be introduced, and its effect on suppressing these resonant peaks that appear in the intended attenuation region will be discussed in Section 4.3. It is also observed that the attenuation pattern exhibits a similar but not identical tendency for $\delta > 0$ and $\delta < 0$. Specifically, attenuation strength is slightly stronger for $\delta > 0$, showing darker colored areas in the low-frequency region and less blank areas in the high-frequency region. **Figure 4(d), (e)** and **(f)** show the attenuation heatmaps for the case of $n = 10$. The length of the $(n+1)$th electrode is $l_{n+1} = 20$ mm, and the total length of the beam is unchanged. Correspondingly, the three groups of inductance are changed to $L = 70.96$ H, $L = 4.44$ H, and $L = 1.45$H to keep the resonant frequency f_{n+1} of the $(n+1)$th shunt resonant circuit to be 100 Hz, 400 Hz, and 700 Hz, respectively. As compared to the cases with $n = 5$, it is confirmed that with the increase of the number of electrode pairs, the vibration attenuation ability is enhanced over a wider frequency range for the graded beam, while the attenuation region remains unchanged for $\delta = 0$. There are two reasons for this. First, dividing the beam into more segments requires more shunt inductors and forms more resonant circuits. It is well-known that increasing the number of local resonators leads to better vibration attenuation performance. Second, as the beam is divided into more segments, the capacitances of those piezoelectric segments become smaller, and larger inductances are needed to achieve the desired resonant frequencies of the shunt circuits. Thus, the counter-moments generated by the inductor shunted piezoelectric segments increase, and the local resonance induced vibration attenuation performance improves.

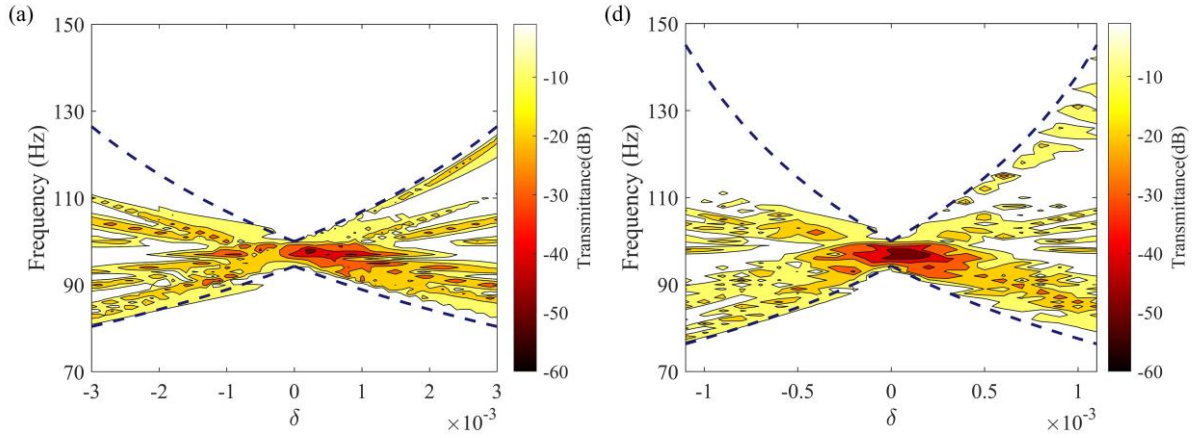

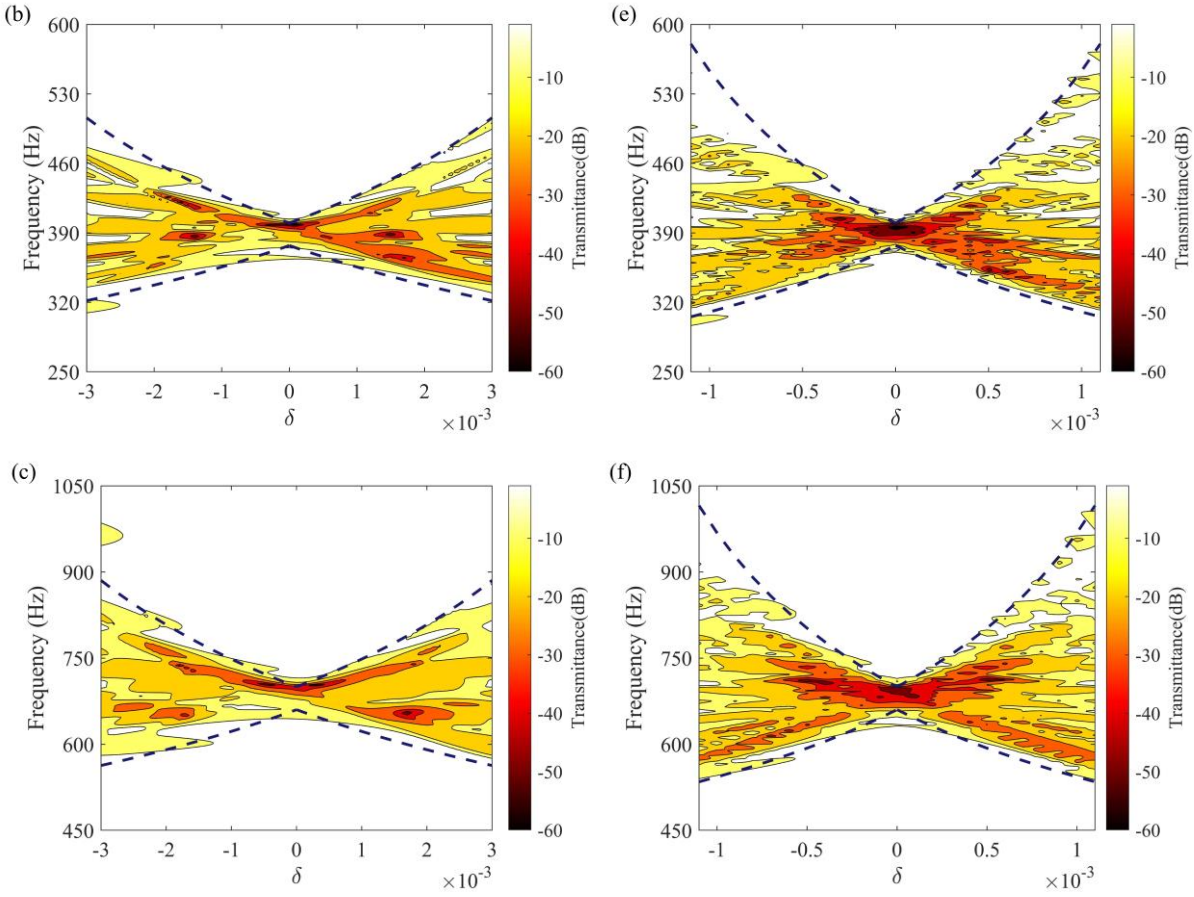

Figure 4. Attenuation heatmaps ($\tau(\omega) < 0$) with varying δ. (a), (b) and (c) represent three cases (i.e., f_{n+1} = 100 Hz, 400 Hz, and 700 Hz, respectively) for n = 5. (d), (e) and (f) represent the three cases for n = 10. The blank area denotes the non-attenuation region ($\tau(\omega) \geq 0$). The dashed lines denote boundaries of the "aggregated" gap estimated by Eq. (21).

To further demonstrate the effect of δ on the attenuation ability of the graded piezoelectric metamaterial beam, **Figure 5** shows the transmittances in six cases of δ with f_{n+1} = 400 Hz and n = 5, which correspond to six slice views of **Figure 4(b)**. The transmittances of the conventional metamaterial beam (δ = 0) are superposed on the plots for comparison.

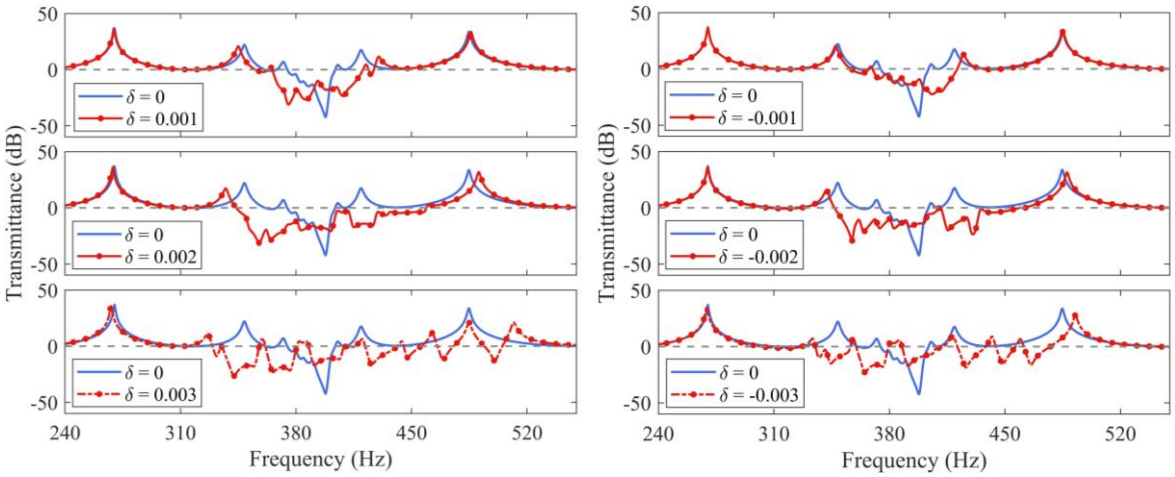

Figure 5. Transmittances of the graded piezoelectric metamaterial beam for different δ ($\pm$ 0.001, $\pm$ 0.002, $\pm$ 0.003). δ = 0 corresponds to the conventional piezoelectric metamaterial beam. n = 5, f_{n+1} = 400 Hz and R = 50 Ω are used.

The trend of the increasing breadth of the valley (i.e., the attenuation region) with the increase of $|\delta|$ is evident in the transmittances. However, as $|\delta|$ continues to increase, the valley is smashed by multiple resonant peaks (cases of $\delta = \pm$ 0.003 in **Figure 5**). Difference between the descending order (i.e., $\delta > 0$) and the ascending order ($\delta < 0$) of the resonant frequencies is observed in the attenuation patterns, which has already been indicated in **Figure 4(b)**. For $\delta > 0$, the valley of the transmittance is slightly deeper in the low-frequency region, especially for δ = 0.001. Meanwhile, the attenuation effect appears at a slightly higher frequency, especially for δ = 0.003. This phenomenon could be attributed to the swapping of the boundary conditions of the two ends of the beam when changing the sign of δ. To be more specific, the above phenomenon can be explained from the following two aspects. On the one hand, the coupling strength between the local resonator and the host beam is position-dependent [42]. Strictly speaking, the position dependence varies with the frequency and the dominant vibration mode. The results in [42] demonstrated that in the low-frequency region, the coupling strength between the local resonator and the host beam gradually increases from the clamped end to the free end [42]. For $\delta > 0$, the piezoelectric segments with lower resonant frequencies are arranged from the free end. This treatment strengthens the couplings of the low-frequency resonators with the host beam. The counter-moments produced by those piezoelectric segments with lower resonant frequencies are increased, thus the vibration suppression capability in the low-frequency region. On the other hand, the lengths of the piezoelectric segments near the clamped end for $\delta > 0$ are shorter than those for $\delta < 0$. Therefore, the capacitances of those segments for $\delta > 0$ are smaller. If the beams in both cases

are under the same deflection, they would have approximately the same stress at the same location. As a result, the voltage outputs from those segments are higher for $\delta > 0$ because of the smaller capacitances. This indicates that a larger counter-moment would be produced by the segments near the clamped end for $\delta > 0$. Therefore, it can be qualitatively known that the beam configuration in the case of $\delta > 0$ should have a higher bending stiffness, and thus its frequency response would be extended toward higher frequencies.

To further compare the vibration attenuation performance of these two grading patterns, **Figure 6** presents the steady-state responses of the graded metamaterial beam with different excitation frequencies using COMSOL. f_{n+1} = 400 Hz, n = 5 and $\delta = \pm 0.001$ are considered, and the excitation frequencies are 365 Hz, 375 Hz, 385 Hz, 395 Hz, 405 Hz, and 415 Hz, falling into the predicted "aggregated" gap (355 Hz to 427 Hz) based on Eq. (21).

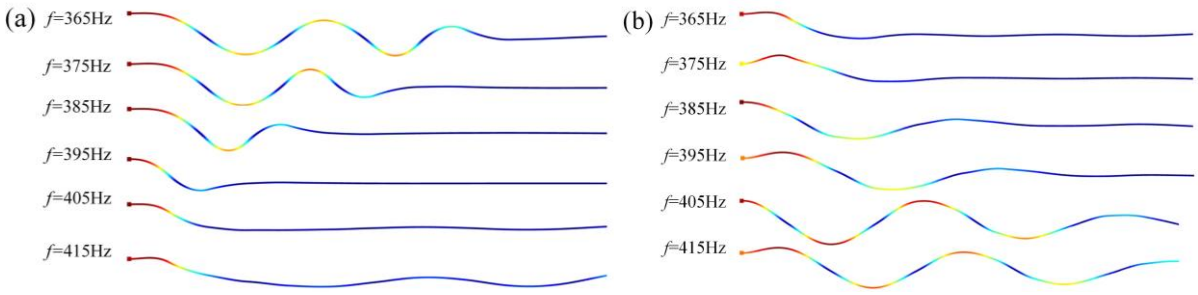

Figure 6. Steady-state response of the graded metamaterial beam at different excitation frequencies (365Hz - 415Hz): (a) δ = 0.001; (b) δ = −0.001. It can be noted in (b) that with the ascending order (δ = −0.001), the propagating waves at higher frequencies (405Hz and 415 Hz) are not sufficiently suppressed.

In the case of $\delta > 0$ (**Figure 6(a)**), it is observed that the transverse wave decays gradually along the beam for the given excitation frequencies. Particularly, waves will be trapped near the clamped end at higher excitation frequencies. These observations match the prediction from the previous analysis. In the case of $\delta < 0$ (**Figure 6(b)**), the vibration pattern is almost reversed, except at higher frequencies where the suppression is not sufficient.

4.2 Optimization Based on Average Transmittance

Based on the analysis in Section 4.1, large attenuation bandwidth can be achieved by increasing the spatial variation δ with the compromised attenuation strength. In many circumstances, vibrational energy predominantly exists in a wide frequency range [43]. For a specific frequency range, researchers have used the average transmittance as an indicator to

optimize the vibration attenuation performance [44]. An average transmittance over the frequency range of interest [ω_l, ω_u] is defined as:

$$\tau_{avg} = \frac{1}{\omega_u - \omega_l}\int_{\omega_l}^{\omega_u} \tau(\omega)\, d\omega \tag{26}$$

The optimization objective is to obtain the minimum average transmittance $\left(\tau_{avg}\right)_{\min}$ by adequately tuning the spatial variation δ. On the other hand, according to the previous analysis, the center frequency of the attenuation region depends on the middle resonant frequency f_{n+1}. If f_{n+1} is outside the targeted frequency range, half or fewer than half of the resonators contribute to the vibration attenuation. Therefore, the variation of f_{n+1} will also be considered in the optimization, and the range of f_{n+1} should be located in $\left[\omega_l / 2\pi, \omega_u / 2\pi\right]$.

Without loss of generality, this study concerns two typical vibration sources: band-limited white noise and band-limited colored noise. Band-limited white noise refers to the noise in which vibration energy is evenly spread certain spectrum, and it can be found in numerous engineering applications [45, 46]. In this study, a frequency range of interest is set from 300 Hz to 500 Hz. 11 electrode pairs (n = 5) are considered, and the other geometric and material parameters are tabulated in **Table 1**.

Figure 7(a) presents the evolution of the average transmittance τ_{avg} for the targeted frequency region with varying δ and f_{n+1}. It is observed that the average transmittance becomes stronger (i.e., τ_{avg} is decreased) with the initial increase of $|\delta|$, while further increasing $|\delta|$ appears to have no benefit or deteriorate the average transmittance. The optimal τ_{avg} occurs at $\delta > 0$, with $\left(\tau_{avg}\right)_{\min} = -7.14$ dB when (δ, f_{n+1}) = (0.0018, 454 Hz), which is slightly better than $\left(\tau_{avg}\right)_{\min} = -5.81$ dB in the case of (δ, f_{n+1}) = (−0.002, 445 Hz). In addition, the optimal average transmittance τ_{avg} = −7.14 dB is reduced more than 66 times as compared to the $\left(\tau_{avg}\right)_{\min} = 0.11$ dB obtained from the conventional piezoelectric metamaterial beam (δ = 0, f_{n+1} = 462 Hz). **Figure 7(b)** describes the evolution of τ_{avg} with varying f_{n+1} given δ = 0, δ = −0.002, and optimal δ=0.0018. The average transmittance of a plain beam without local resonances (i.e., all the piezoelectric segments are short-circuited) is also superposed on the plot. **Figure 8** compares the transmittance response of the graded and the conventional piezoelectric metamaterial beams with their corresponding optimal cases. These results

further confirm the superiority of the graded design as compared to the conventional non-graded piezoelectric metamaterial beam.

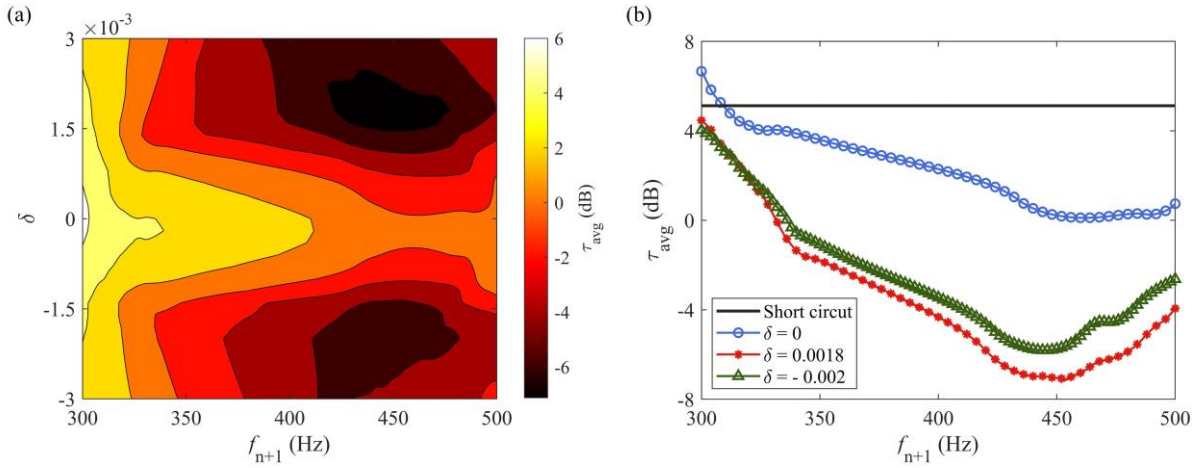

Figure 7. Evolution of average transmittance τ_{avg} in the case of white noise excitation. (a) Heatmap of τ_{avg} with varying δ and f_{n+1}; (b) τ_{avg} with varying f_{n+1} for δ = 0, −0.002, 0.0018 and short-circuit condition (plain beam). n = 5 and R = 50 Ω are used.

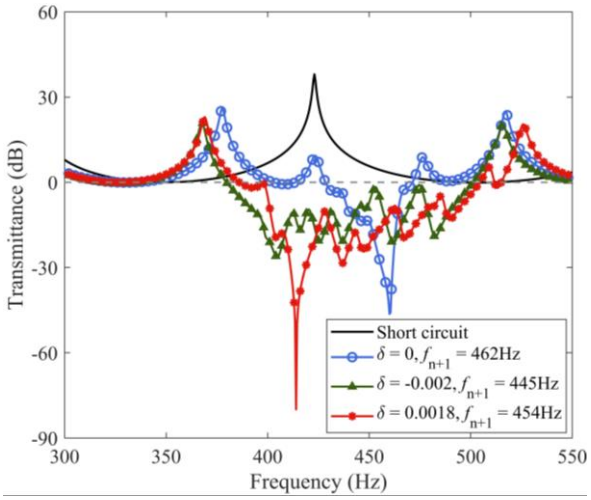

Figure 8. Transmittances for the cases with δ = 0, −0.002, 0.0018 and short-circuit condition (plain beam). n = 5 and R = 50 Ω are used.

Next, the evolution of the average transmittance τ_{avg} in the case of colored noise excitation is investigated. Colored noise refers to the noise in which the power spectral density is not flat in the spectrum [47]. Without loss of generality, we take the dominant frequency range of the vibration acceleration spectrum of a rail track [48] as an example, whose spectrum profile is close to a Gaussian distribution that can be found in many vibration/noise environments [49, 50]. To make the optimization process concise, the spectrum of the signal in [48] is approximated as:

$$\chi(\omega) = \lambda^3 (\omega - \omega_l)^3 (\omega_u - \omega_l - (\omega - \omega_l))^3 \tag{27}$$

$[\omega_l, \omega_u]$ is the targeted frequency range. Eq. (27) is normalized by dividing its maximum value, which yields $\tilde{\chi}(\omega) = \chi(\omega) / (\chi(\omega))_{\max}$. By reference to Figure 3 in [48], the targeted frequency range is chosen as [200 Hz, 300 Hz], and λ is roughly identified as 0.0007, leading to the spectrum shown in **Figure 9**. Since the proposed graded metamaterial beam modeled by the Euler-Bernoulli beam theory is a linear system, the influence of the colored noise excitation is reflected by multiplying $\tilde{\chi}(\omega)$ to Eq. (26)

$$\tau_{avg,c} = \frac{1}{\omega_u - \omega_l} \int_{\omega_l}^{\omega_u} \tilde{\chi}(\omega) \tau(\omega) d\omega \tag{28}$$

The subscript c denotes the case of color noise excitation. The range of the resonant frequency f_{n+1} of the shunt circuit connected to the middle piezoelectric segment is set to be within [200 Hz, 300 Hz]. **Figure 10(a)** shows the evolution of $\tau_{avg,c}$ with varying δ and f_{n+1}. Again, the optimal $\tau_{avg,c}$ is obtained in the grading pattern of $\delta > 0$, which is $(\tau_{avg})_{\min} = -7.01$ dB when (δ, f_{n+1}) = (0.0014, 259 Hz).

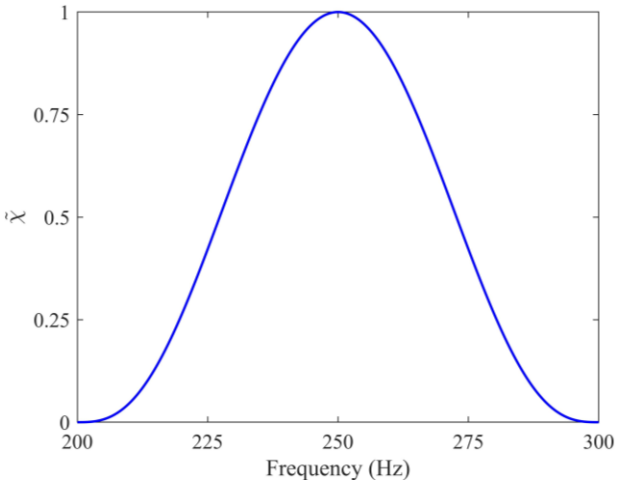

Figure 9. A normalized spectrum of colored noise excitation by reference to the acceleration spectrum of a rail track in [48], which is close to a Gaussian distribution.

For $\delta < 0$, the optimal $\tau_{avg,c}$ is −5.14 dB when (δ, f_{n+1}) = (−0.0014, 256 Hz), which is slightly weaker than $\delta > 0$. In addition, the average transmittance values in the optimal cases of the graded metamaterial beam with two grading patterns show significant improvement as compared to that of the conventional metamaterial($(\tau_{avg})_{\min} = -1.58$ dB at (δ = 0, f_{n+1} = 257 Hz)). **Figure 10(b)** shows the variation of $\tau_{avg,c}$ with varying f_{n+1} given δ = 0, δ = 0.0014 and δ = −0.0014. The average transmittance of the plain beam (i.e., all the piezoelectric segments are short-circuited) is also plotted in **Figure 10(b)** for comparison. It can be found that the

optimal f_{n+1} occurs at the maximum amplitude of the interested frequency spectrum. For other vibration sources with different spectrums, one can optimize the graded metamaterial beam using the same approach proposed in this section. With the optimal parameter settings, a comparison of the transmittances of the plain beam, conventional metamaterial beam, and graded metamaterial beam is shown in **Figure 11.** Notable vibration reduction with the graded metamaterial beam can be observed in the interested frequency range.

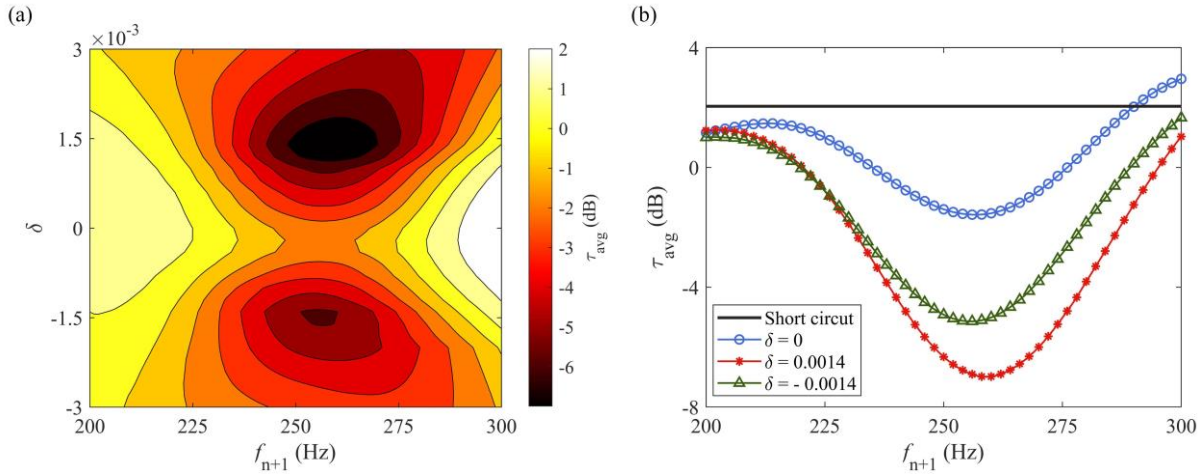

Figure 10. Evolution of average transmittance τ_{avg} in the case of colored noise excitation. (a) Heatmap of τ_{avg} with varying δ and f_{n+1}; (b) τ_{avg} with varying f_{n+1} for δ = 0, 0.0014, −0.0014 and short-circuit condition (plain beam). n = 5 and R = 50 Ω are used.

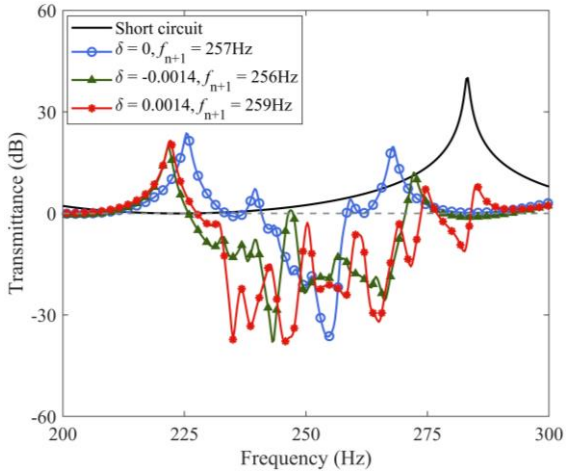

Figure 11. Transmittances for the cases with δ = 0, −0.0014, 0.0014 and short-circuit condition (plain beam). n = 5 and R = 50 Ω are used.

4.3 Elimination of Localization Induced Resonant Peaks

The previous analysis shows that the proposed graded piezoelectric metamaterial beam can improve the attenuation bandwidth and the average transmittance, as compared to the conventional piezoelectric metamaterial beam without grading. However, the presence of

resonant peaks due to localized mode in the intended "aggregated" gap undermines the broadband vibration attenuation. It is known that resonant peaks can be eliminated by using larger damping. Here, the effect of modal damping ratio ζ_r, which actually introduces global damping to the beam is studied. For n = 5, R = 1 Ω, f_{n+1} = 400 Hz, and δ = 0.002, **Figure 12** shows the transmittances as ζ_r increases. It is found that some resonant peaks inside the predicted "aggregated" gap are insensitive to ζ_r. Resonant peaks are still prominent even with a large ζ_r.

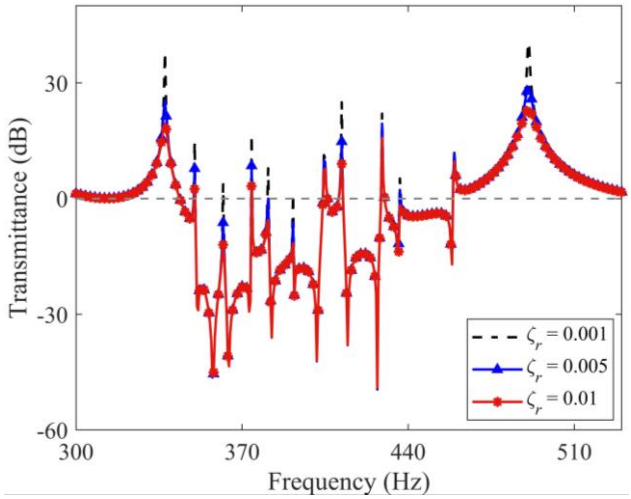

Figure 12. Transmittances of the graded piezoelectric metamaterial beam with different ζ_r. n = 5, δ = 0.002, f_{n+1} = 400 Hz and R = 1 Ω are used.

In [51], the metamaterial beam attached with pure mechanical resonators was studied. The conclusion drawn from [51] indicates that the material damping of the local resonators strongly affects the transmittance response inside the bandgap locally. According to the analogy between electrical and mechanical domains, the load resistance in the shunt resonant circuit plays the role of damping. Hence, by reference to [51], we anticipate that the load resistance may also directly affect the resonant peaks within the attenuation region and is therefore studied in this section. Note that the attenuation zone of the graded metamaterial beam typically contains multiple discrete gaps. To evaluate the width of the attenuation region, a dominant attenuation bandwidth $\Delta\omega_D$ is defined, which describes the largest continuous bandwidth with $\tau(\omega) < 0$ in the designed "aggeragated" gap. ω_D^+ and ω_D^- are the upper and lower bounds of $\Delta\omega_D$. For ζ_r = 0.001, n = 5, f_{n+1} = 400 Hz and δ = 0.002, **Figure 13(a)** shows the variation of $\Delta\omega_D$ of the graded piezoelectric metamaterial beam when R varies. The "aggregated" gap estimated by Eq. (21) is shaded in grey as a reference. The

relative error (defined as $\left|\omega_D^+ - \omega^+\right| / \omega^+ + \left|\omega_D^- - \omega^-\right| / \omega^-$) is plotted in **Figure 13(a)**, where ω^+ and ω^- respectively denote the upper and lower bounds of the designed "aggregated" gap. It can be seen in **Figure 13(a)** that when R is large enough, $\Delta\omega_D$ matches the designed "aggregated" gap, which, as discussed in Section 3, is an ideal overlapping bandgap and is the widest gap that can theoretically be obtained by grading. It is noteworthy that this continuous gap is a pseudo bandgap since the bandgap is normally defined based on the band structure analysis (i.e., the blank area represented by the complex Bloch wavenumbers, which indicates the evanescent waves).

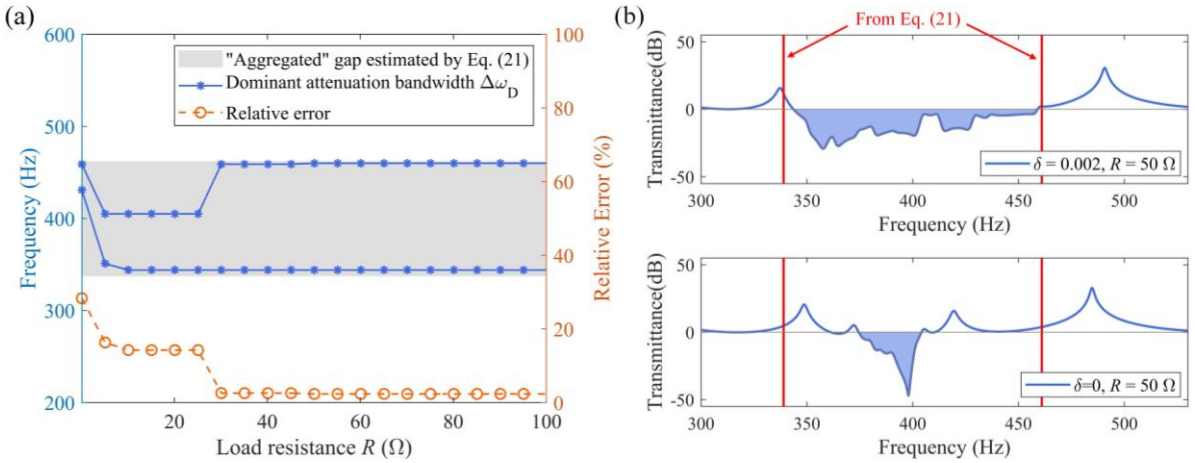

Figure 13. (a) Comparison of the dominant attenuation bandwidth $\Delta\omega_D$ and the "aggregated" gap estimated by Eq. (21) for the graded piezoelectric metamaterial beam with varying R. Note that $\Delta\omega_D$ gradually approaches the "aggregated" gap with the increase of R; (b) Comparison of $\Delta\omega_D$ between the graded piezoelectric metamaterial beam (δ = 0.002) and conventional piezoelectric metamaterial beam (δ = 0) with a proper R. The color-filled area denotes $\Delta\omega_D$.

The transmittance of the graded piezoelectric metamaterial beam with a proper load resistance (R = 50 Ω) is given in **Figure 13(b)**, in which the region with $\tau(\omega) < 0$ (i.e., the pseudo bandgap) is shaded in blue. Clearly, the shaded area (ranges from 343.6 Hz to 459.0 Hz) of the graded piezoelectric metamaterial beam is consistent with the estimation from Eq. (21) (ranges from 337.4 Hz to 461.8 Hz). For a direct comparison, the transmittance of the conventional non-graded piezoelectric metamaterial beam with the same load resistance is also shown in **Figure 13(b)**, which creates a narrow bandgap (ranges from 374.5Hz to 404.1Hz). It can be seen that the graded beam achieves a 289.2% enlargement of the attenuation bandwidth as compared to the conventional one.

In addition, it should be pointed out that the precision of the predicted response relies on the accuracy of the system parameters. In practical applications, the manufacturing tolerances associated with the mechanical/electrical properties are inevitable, making it challenging to achieve a rigorous grading design. Therefore, the robustness of the grading design is worth investigation. Here, we consider the uncertainties of the inductance L in the shunt circuit since the inductance value determines the resonant frequency and will directly affect the attenuation performance. To quantify the uncertainty, a tolerance of $\pm 10\%$ is adopted in the following analysis, which is a common value reported in [52, 53]. The realistic inductance L_j of the jth shunt circuit is assigned as

$$L_j = \left(1+\gamma_j\right)L \tag{29}$$

where γ_j is a stochastic deviation randomly generated between −10% and +10%. For n = 5, R = 50 Ω, f_{n+1} = 400 Hz, δ = 0.002, **Figure 14(a)** compares the transmittances of the graded piezoelectric metamaterial beam with the nominal inductors and with the realistic inductors. Five sets of randomly generated inductors are used for comparison, and the deviation of each inductor is listed in **Table 2**.

Table 2. Stochastic deviation for the inductors in the shunt circuits.

	γ_1(%)	γ_2(%)	γ_3(%)	γ_4(%)	γ_5(%)	γ_6(%)	γ_7(%)	γ_8(%)	γ_9(%)	γ_{10}(%)	γ_{11}(%)
Case 1	−3.5	3.4	−1.2	6.7	5.4	−6.7	7.2	9.8	0.3	7.7	1.8
Case 2	−5.9	−7.1	−6.2	−9.2	2.7	−4.4	0.8	3.9	−0.02	0.7	−1.1
Case 3	−0.04	8.0	1.5	6.9	4.8	1.7	−5.1	3.3	−8.3	2.5	3.2
Case 4	7.2	8.7	9.7	7.2	5.7	0.3	−6.5	−2.0	−7.2	−9.4	8.8
Case 5	−4.0	−4.1	−3.3	−0.7	3.0	−9.5	6.8	1.1	7.1	−3.0	−1.1

It can be seen that the targeted location of the attenuation region is insensitive to the uncertainty, but the transmittance within the attenuation region becomes more uneven. This is because the design criterion for the formation of “aggregated” gap is more difficult to guarantee with the slightly varying inductors.

According to the previous analysis in this subsection, a larger resistance is beneficial to eliminate resonant peaks, and could thus potentially improve the grading design’s robustness. With the same parameters, **Figure 14(b)** shows the transmittance response with R = 300 Ω. It can be found that the transmittance responses become smoothened, and the discrepancy between the cases of nominal inductors and realistic inductors becomes acceptable, implying that broadband vibration attenuation can still be achieved even with uncertainties of circuitry parameters.

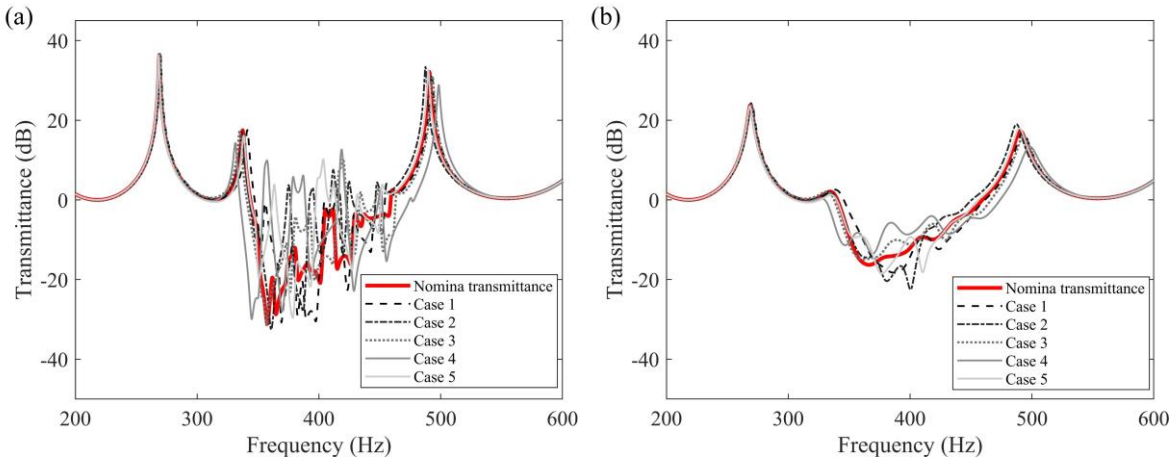

Figure 14. Transmittance comparison of the graded piezoelectric metamaterial beam between nominal prediction and different realizations with uncertainties in the inductors listed in **Table 2**: (a) R = 50 Ω; (b) R = 300 Ω. n = 5, δ = 0.002, and f_{n+1} = 400 Hz are used.

5. Conclusions

This paper presents a novel graded piezoelectric metamaterial beam with shunt resonant circuits for broadband vibration attenuation. A grading strategy of spatial variation of electrode pairs has been proposed. The design criterion is derived, and an explicit expression for the lower and upper bounds of the "aggregated" gap region is obtained. The theoretical transmittance results of the proposed metamaterial beam have been verified by finite element analysis showing a high consistency.

Based on the established theoretical models and the derived design criterion, the vibration attenuation performance of the proposed system has been comprehensively investigated. It is found that increasing the spatial variation δ of the electrode pairs leads to profound changes in wave attenuation characteristics: The bandgap in the conventional non-graded piezoelectric metamaterial beam is spread out into a wider but scattered frequency bandwidth, accompanied by a decrease of the attenuation strength. With this understanding, the graded piezoelectric metamaterial beam is optimized in terms of average attenuation strength, which shows superior performance of the proposed graded design in the prescribed frequency spectrum as compared to the conventional non-graded one. Moreover, some undesired characteristics, e.g., multiple resonant peaks inside the attenuation region, and the uncertainties of the circuitry parameters, can be mitigated by adequately tuning the load resistance in the shunt resonant circuit. Theoretical widest attenuation region can be realized with a decent load resistance, matching the estimated "aggregated" gap.

This work provides a new avenue to realize broadband wave and vibration attenuation through the design of the spatial variation of properties in a metamaterial system.

Acknowledgments

This work was financially supported by a PhD scholarship from the China Scholarship Council (No. 201907000126) and the Faculty Research Development Fund from the University of Auckland (No. 3722094).

References

[1] Chang I-L, Liang Z-X, Kao H-W, Chang S-H, Yang C-Y. The wave attenuation mechanism of the periodic local resonant metamaterial. Journal of Sound and Vibration. 2018;412:349-59.
[2] Butt H, Dai Q, Farah P, Butler T, Wilkinson TD, Baumberg JJ, et al. Metamaterial high pass filter based on periodic wire arrays of multiwalled carbon nanotubes. Applied physics letters. 2010;97:163102.
[3] Trainiti G, Xia Y, Marconi J, Cazzulani G, Erturk A, Ruzzene M. Time-periodic stiffness modulation in elastic metamaterials for selective wave filtering: Theory and experiment. Physical review letters. 2019;122:124301.
[4] Guell Izard A, Valdevit L. Magnetoelastic metamaterials for energy dissipation and wave filtering. Advanced Engineering Materials. 2020;22:1901019.
[5] Zhang Q, Guo D, Hu G. Tailored Mechanical Metamaterials with Programmable Quasi-Zero-Stiffness Features for Full-Band Vibration Isolation. Advanced Functional Materials. 2021:2101428.
[6] Li Y, Baker E, Reissman T, Sun C, Liu WK. Design of mechanical metamaterials for simultaneous vibration isolation and energy harvesting. Applied Physics Letters. 2017;111:251903.
[7] Cai C, Wang Z, Chu Y, Liu G, Xu Z. The phononic band gaps of Bragg scattering and locally resonant pentamode metamaterials. Journal of Physics D: Applied Physics. 2017;50:415105.
[8] Liu K, Liu J. The damped dynamic vibration absorbers: revisited and new result. Journal of sound and vibration. 2005;284:1181-9.
[9] Li G, Chen Y, Chen W, Liu J, He H. Local resonance–Helmholtz lattices with simultaneous solid-borne elastic waves and air-borne sound waves attenuation performance. Applied Acoustics. 2022;186:108450.
[10] Pai PF. Metamaterial-based broadband elastic wave absorber. Journal of Intelligent Material Systems and Structures. 2010;21:517-28.
[11] Xiao Y, Wen J, Wen X. Broadband locally resonant beams containing multiple periodic arrays of attached resonators. Physics Letters A. 2012;376:1384-90.
[12] Zhu R, Liu XN, Hu GK, Sun CT, Huang GL. A chiral elastic metamaterial beam for broadband vibration suppression. Journal of Sound and Vibration. 2014;333:2759-73.
[13] Yu D, Liu Y, Zhao H, Wang G, Qiu J. Flexural vibration band gaps in Euler-Bernoulli beams with locally resonant structures with two degrees of freedom. Physical Review B. 2006;73:064301.
[14] Xiao Y, Wen J, Wen X. Longitudinal wave band gaps in metamaterial-based elastic rods containing multi-degree-of-freedom resonators. New Journal of Physics. 2012;14:033042.
[15] Hu G, Tang L, Das R. Internally coupled metamaterial beam for simultaneous vibration suppression and low frequency energy harvesting. Journal of Applied Physics. 2018;123:055107.
[16] Zhou W, Wu Y, Zuo L. Vibration and wave propagation attenuation for metamaterials by periodic piezoelectric arrays with high-order resonant circuit shunts. Smart Materials and Structures. 2015;24:065021.
[17] Wang G, Chen S. Large low-frequency vibration attenuation induced by arrays of piezoelectric patches shunted with amplifier–resonator feedback circuits. Smart Materials and Structures. 2015;25:015004.

[18] Wang G, Cheng J, Chen J, He Y. Multi-resonant piezoelectric shunting induced by digital controllers for subwavelength elastic wave attenuation in smart metamaterial. Smart Materials and Structures. 2017;26:025031.
[19] Wang G, Wang J, Chen S, Wen J. Vibration attenuations induced by periodic arrays of piezoelectric patches connected by enhanced resonant shunting circuits. Smart Materials and Structures. 2011;20:125019.
[20] Li X, Chen Y, Hu G, Huang G. A self-adaptive metamaterial beam with digitally controlled resonators for subwavelength broadband flexural wave attenuation. Smart Materials and Structures. 2018;27:045015.
[21] Baz A. Active acoustic metamaterial with tunable effective density using a disturbance rejection controller. Journal of Applied Physics. 2019;125:074503.
[22] Krushynska AO, Miniaci M, Bosia F, Pugno NM. Coupling local resonance with Bragg band gaps in single-phase mechanical metamaterials. Extreme Mechanics Letters. 2017;12:30-6.
[23] Sugino C, Ruzzene M, Erturk A. Merging mechanical and electromechanical bandgaps in locally resonant metamaterials and metastructures. Journal of the Mechanics and Physics of Solids. 2018;116:323-33.
[24] Wen S, Xiong Y, Hao S, Li F, Zhang C. Enhanced band-gap properties of an acoustic metamaterial beam with periodically variable cross-sections. International Journal of Mechanical Sciences. 2020;166:105229.
[25] Xiao Y, Mace BR, Wen J, Wen X. Formation and coupling of band gaps in a locally resonant elastic system comprising a string with attached resonators. Physics Letters A. 2011;375:1485-91.
[26] Luongo A. Mode localization by structural imperfections in one-dimensional continuous systems. Journal of sound and vibration. 1992;155:249-71.
[27] Asatryan AA, Botten LC, Byrne MA, Freilikher VD, Gredeskul SA, Shadrivov IV, et al. Suppression of Anderson localization in disordered metamaterials. Physical review letters. 2007;99:193902.
[28] Shao H, Chen G, He H. Elastic wave localization and energy harvesting defined by piezoelectric patches on phononic crystal waveguide. Physics Letters A. 2021;403:127366.
[29] Banerjee A, Das R, Calius EP. Frequency graded 1D metamaterials: a study on the attenuation bands. Journal of Applied Physics. 2017;122:075101.
[30] Hu G, Austin AC, Sorokin V, Tang L. Metamaterial beam with graded local resonators for broadband vibration suppression. Mechanical Systems and Signal Processing. 2021;146:106982.
[31] Alshaqaq M, Erturk A. Graded multifunctional piezoelectric metastructures for wideband vibration attenuation and energy harvesting. Smart Materials and Structures. 2020;30:015029.
[32] Celli P, Yousefzadeh B, Daraio C, Gonella S. Bandgap widening by disorder in rainbow metamaterials. Applied Physics Letters. 2019;114:091903.
[33] Sugino C, Xia Y, Leadenham S, Ruzzene M, Erturk A. A general theory for bandgap estimation in locally resonant metastructures. Journal of Sound and Vibration. 2017;406:104-23.
[34] Bhaskar D, Senani R. Synthetic floating inductors realized with only two current feedback op-amps. American Journal of Electrical and Electronic Engineering. 2015;3:88-92.
[35] Sugino C, Leadenham S, Ruzzene M, Erturk A. An investigation of electroelastic bandgap formation in locally resonant piezoelectric metastructures. Smart Materials and Structures. 2017;26:055029.
[36] Jian Y, Hu G, Tang L, Xu J, Aw KC. A generic theoretical approach for estimating bandgap bounds of metamaterial beams. Journal of Applied Physics. 2021;130:054501.
[37] Shengbing C, Jihong W, Gang W, Dianlong Y, Xisen W. Improved modeling of rods with periodic arrays of shunted piezoelectric patches. Journal of Intelligent Material Systems and Structures. 2012;23:1613-21.
[38] El-Borgi S, Fernandes R, Rajendran P, Yazbeck R, Boyd J, Lagoudas D. Multiple bandgap formation in a locally resonant linear metamaterial beam: Theory and experiments. Journal of Sound and Vibration. 2020;488:115647.
[39] Thorp O, Ruzzene M, Baz A. Attenuation and localization of wave propagation in rods with periodic shunted piezoelectric patches. Smart Materials and Structures. 2001;10:979.

[40] Yi K, Ouisse M, Sadoulet-Reboul E, Matten G. Active metamaterials with broadband controllable stiffness for tunable band gaps and non-reciprocal wave propagation. Smart Materials and Structures. 2019;28:065025.
[41] Chaplain GJ, Pajer D, De Ponti JM, Craster RV. Rainbow reflection and trapping for energy harvesting. arXiv preprint arXiv:200205260. 2020.
[42] Hu G, Wang J, Tang L. A comb-like beam based piezoelectric system for galloping energy harvesting. Mechanical Systems and Signal Processing. 2021;150:107301.
[43] Vér IL, Beranek LL. Noise and vibration control engineering: principles and applications: John Wiley & Sons; 2005.
[44] Meng H, Chronopoulos D, Fabro AT, Maskery I, Chen Y. Optimal design of rainbow elastic metamaterials. International Journal of Mechanical Sciences. 2020;165:105185.
[45] Ardekani IT, Abdulla WH. On the convergence of real-time active noise control systems. Signal Processing. 2011;91:1262-74.
[46] Hirai T, Uematsu T, Sasaki Y, Toda M. Dynamic responses of nailed plywood-timber joints under a band-limited white-noise wave. Journal of wood science. 2013;59:477-83.
[47] Zhivomirov H. A method for colored noise generation. Romanian journal of acoustics and vibration. 2018;15:14-9.
[48] Burdzik R, Konieczny Ł, Nowak B, Rozmus J. Research on vibration employed for the train traffic control. Vibroengineering PROCEDIA. 2017;14:227-32.
[49] Ma M, Jiang B, Liu W, Liu K. Control of metro train-induced vibrations in a laboratory using periodic piles. Sustainability. 2020;12:5871.
[50] Li H, Zhang X, Xu F. Experimental investigation on centrifugal compressor blade crack classification using the squared envelope spectrum. Sensors. 2013;13:12548-63.
[51] Hu G, Xu J, Tang L, Lan C, Das R. Tunable metamaterial beam using negative capacitor for local resonators coupling. Journal of Intelligent Material Systems and Structures. 2020;31:389-407.
[52] Ruiz RO, Meruane V. Uncertainties propagation and global sensitivity analysis of the frequency response function of piezoelectric energy harvesters. Smart Materials and Structures. 2017;26:065003.
[53] Pan W, Tang G, Tang J. Evaluation of uncertainty effects to band gap behavior of circuitry-integrated piezoelectric metamaterial using order-reduced analysis. Journal of Intelligent Material Systems and Structures. 2018;29:2677-92.